Indian Journal of Chemistry
Vol. 62, October 2023, pp. 1081-1090
DOI: 10.56042/ijc.v62i10.6188

Synthesis, structural characterization and Hirshfeld surface analysis of copper(I) complexes containing hemilabile-ferrocenylbisphosphine [Fe{$C_5H_4P(C_6H_4CH_2NMe_2$-*o*)$_2$}$_2$]

Dipanjan Mondal[a], Sowmya Rao[a], Joel T Mague[b] & Maravanji S Balakrishna*[a]

[a] Phosphorus Laboratory, Department of Chemistry, Indian Institute of Technology Bombay, Powai, Mumbai 400 076, India

[b] Department of Chemistry, Tulane University, New Orleans, Louisiana 70118, USA

E-mail: joelt@tulane.edu, krishna@chem.iitb.ac.in

Received 16 January 2023; accepted (revised) 21 September 2023

The reactions of ferrocenylbisphosphine, [Fe{$C_5H_4P(C_6H_4CH_2NMe_2$-*o*)$_2$}$_2$] (**1**) comprising dangling amine functionalities with CuX yielded dinuclear complexes [{$Cu_2(\mu$-X)$_2$}{Fe($C_5H_4P(C_6H_4CH_2NMe_2$-*o*)$_2$)$_2$}] (**2**, X = Cl; **3**, X = Br; **4** X = I). The reaction of **4** with pyridine affords a binuclear complex, [{Cu_2I_2(py)$_2$}{Fe($C_5H_4P(C_6H_4CH_2NMe_2$-*o*)$_2$)$_2$}] (**5**) (py = pyridine) in which each copper atom is tetracoordinated. Similarly, treatment of **4** with 2,2'-bipyridine in 1:1 molar ratio afforded the binuclear complex, [{Cu_2I_2(2,2′-bipy)}{Fe-($C_5H_4P(C_6H_4CH_2NMe_2$-*o*)$_2$)$_2$}] (**6**). The equimolar reaction of **3** and 4,4′-bipyridine affords [{Cu_2Br_2(4,4′-bipy)}$_2$Fe(C_5H_4P- ($C_6H_4CH_2NMe_2$-*o*)$_2$)$_2$}$_2$] (**7**) in good yield. The complexes **2** and **4** have been structurally characterized; both crystallize in the monoclinic space group with C2/c. In the crystal packing of **2** and **4**, the invention-related intermolecular C-H···X (X = Cl and I) and C-H···π(ring) interactions are primarily responsible for the crystal packing. A Hirshfeld surface analysis indicates that the most significant contributions to the crystal packing of **2** are from H···H (81.7%), C···H/H···C (12.4%), Cl···H/H···Cl (4.3%) contacts, while those for **4** are from H···H (80.9%), C···H/H···C (12.1%), I···H/H···I (5.4%) contacts.

Keywords: Ferrocenylbisphosphine, Copper complexes, Crystal structure, Hirshfeld surface analysis, Dangling amines

In recent years, the chemistry of copper(I) complexes has drawn considerable attention due to their interesting structural features, photophysical properties and catalytic applications[1]. The considerable versatility in the structural features of copper(I) complexes is due to the remarkable ability of CuX fragments to assemble in a variety of modes to generate dinuclear rhombus, trinuclear trigonal planar, tetranuclear square planes, cubanes, stair steps or ladders, besides several 1D, 2D or 3D coordination polymers[2,3]. The structural preference depends on the metal-to-ligand ratios, steric properties of the ligands and also their bite separations. Short bite ligands prefer dinuclear to tetranuclear structures, whereas the large bite ligands adopt cubane or ladder structures. Our group has generated a library of phosphorus-based ligands[3-10], in particular P,N-donor ligands[11-18] and studied extensively the coordination chemistry, and photophysical properties of copper(I) complexes. Our group also reported the synthesis and transition metal chemistry of several P,N-donor and ferrocene-based phosphorus ligands, because of their unique coordination properties, as well as catalytic potential in a variety of organic transformations[5,19-23]. We recently reported the synthesis and metal chemistry of [Fe{$C_5H_4P(C_6H_4CH_2NMe_2$-*o*)$_2$}$_2$] (**1**)[24,25]. In this paper, the synthesis and structural characterization of three copper(I) complexes containing ferrocenylbis-phosphine [Fe{$C_5H_4P(C_6H_4CH_2NMe_2$-*o*)$_2$}$_2$] (**1**) with amine functionalities is described.

Experimental Section

Synthesis and crystallization

All experimental manipulations were performed using standard vacuum-line and Schlenk techniques under nitrogen atmosphere unless otherwise stated. All the solvents were purified by conventional procedures and distilled prior to use. Bisphosphine [Fe{$C_5H_4P(C_6H_4CH_2NMe_2$-*o*)$_2$}$_2$] (**1**) was prepared according to the published procedure[24]. CuI was purchased from Sigma Aldrich and used as received. Pyridine, 2,2′-bipyridine (2,2′-bipy) and 4,4′-bipyridine (4,4′-bipy) were purchased from S.D fine Chemicals, India, and purified prior to use, by conventional methods. CuX (X = Cl, Br)[26] were prepared according to the published procedures.

Synthesis of [{Cu_2(μ-Cl)$_2$}{Fe(C_5H_4P($C_6H_4CH_2NMe_2$-*o*)$_2$)$_2$}] (2)

A solution of CuCl (0.015 g, 0.153 mmol) in acetonitrile (4 mL) was added drop-wise to a solution of **1** (0.060 g, 0.077 mmol) in dichloromethane (6 mL). The reaction mixture was allowed to stir at RT for 8 h. The resulting yellow solution was concentrated to 3 mL followed by the addition of petroleum ether to give a yellow precipitate of **2**. Pale yellow crystals were obtained upon recrystallization from a 1:1 dichloromethane/petroleum ether mixture. Yield 81% (0.048 g). m.p. 210-212 °C (dec). $^{31}P\{^1H\}$NMR ($CDCl_3$): δ -38.3 (s). ^1H NMR ($CDCl_3$): δ 2.42 (br s, NMe_2, 24H), 3.33-3.61 (m, CH_2, 8H), 4.58 (br s, 4H, Fc), 7.36-7.55 (m, ArH, 16H). Anal. Calcd for $C_{46}H_{56}N_4P_2FeAu_2Cl_2$: C, 44.28; H, 4.52; N, 4.49%. Found: C, 43.98; H, 4.97; N, 4.52%.

Synthesis of [{Cu_2(μ-Br)$_2$}{Fe(C_5H_4P($C_6H_4CH_2NMe_2$-*o*)$_2$)$_2$}] (3)

This was synthesized by a procedure analogous to **2** using ligand **1** (0.040 g, 0.051 mmol) and CuBr (0.015 g, 0.102 mmol). Yield 83% (0.045 g). m.p. >220 °C (dec). $^{31}P\{^1H\}$NMR ($CDCl_3$): δ -17.2 (s). ^1H NMR ($CDCl_3$): δ 1.70 (br s,NMe_2, 12H), 2.42 (br s, NMe_2, 12H), 3.42-3.59 (m, CH_2, 8H), 4.75 (br s, 4H, Fc), 7.44-7.62 (m, ArH, 16H). Anal. Calcd for $C_{46}H_{56}N_4P_2FeCu_2Br_2.CH_2Cl_2$: C, 48.89; H, 5.06; N, 4.85%. Found: C, 48.93; H, 5.17; N, 4.63%.

Synthesis of [{Cu_2(μ-I)$_2$}{Fe(C_5H_4P($C_6H_4CH_2NMe_2$-*o*)$_2$)$_2$}] (4)

This was synthesized by a procedure similar to **2** using ligand **1** (0.039 g, 0.050 mmol) and CuI (0.019 g, 0.101 mmol). Yield 59% (0.034 g). m.p. >220 °C (dec). Anal. Calcd for $C_{46}H_{56}N_4P_2FeCu_2I_2$: C, 47.48; H, 4.85; N, 4.81%. Found: C, 47.88; H, 4.77; N, 4.58%.

Synthesis of [{Cu_2I_2(py)$_2$}{Fe(C_5H_4P($C_6H_4CH_2NMe_2$-*o*)$_2$)$_2$}] (5)

To 5 mL of pyridine, compound **4** (0.016 g, 0.014 mmol) was added and allowed to stir at RT for 6 h. The resulting yellow solution was dried under vacuum, the residue was dissolved in dichloromethane and layered with petroleum ether and stored at –10 °C to give yellow crystalline product **5**. Yield 65% (0.012 g). m.p. >200 °C (dec). $^{31}P\{^1H\}$NMR ($CDCl_3$): δ -18.4 (br s). ^1H NMR ($CDCl_3$): δ 1.98 (br s, NMe_2, 24H), 3.03-3.35 (m, CH_2, 8H), 4.05 (s, 4H, Fc), 4.24 (s, 4H, Fc), 7.30-7.55 (m, ArH, 16H), 7.64-8.43 (m, Py-H, 10H). Anal. Calcd for $C_{56}H_{66}N_6P_2FeCu_2I_2$: C, 50.88; H, 5.03; N, 6.36%. Found: C, 49.83; H, 4.99; N, 6.55%.

Synthesis of [{Cu_2I_2(2,2′-bipy)}{Fe(C_5H_4P($C_6H_4CH_2NMe_2$-*o*)$_2$)$_2$}] (6)

To a turbid solution of **4** (0.016 g, 0.014 mmol) in dichloromethane (5 mL), was added drop-wise a solution of 2,2'-bipyridine (0.002 g, 0.014 mmol) in the same solvent (5 mL) and the reaction mixture was stirred at RT for 4 h till the solution became clear. The resulting yellow solution was concentrated and kept at RT for 1 day to give analytically pure bright yellow product **6**. Yield 86% (0.016 g). m.p. >200 °C (dec). $^{31}P\{^1H\}$NMR ($CDCl_3$): δ -18.9 (br s). ^1H NMR ($CDCl_3$): δ 2.07 (br s, NMe_2, 24H), 3.23-3.39 (m, CH_2, 8H), 4.06 (br s, 4H, Fc), 4.77 (br s, 4H, Fc), 7.43-7.51 (m, ArH, 16H), 7.54-8.13 (m, Pyr-H, 8H). Anal. Calcd for $C_{56}H_{64}N_6P_2FeCu_2I_2$: C, 50.96; H, 4.89; N, 6.37%. Found: C, 51.33; H, 4.74; N, 6.12%.

Synthesis of [{Cu_2Br_2(4,4′-bipy)}$_2$}{Fe(C_5H_4P($C_6H_4CH_2NMe_2$-*o*)$_2$)$_2$}$_2$] (7)

This was synthesized by a procedure similar that of **6** using complex **3** (0.020 g, 0.019 mmol) and 4,4'-bipyridine (0.003 g, 0.019 mmol). Yield 79% (0.037 g). m.p. >220 °C (dec). $^{31}P\{^1H\}$NMR ($CDCl_3$): δ -13.9 (br s). ^1H NMR ($CDCl_3$): δ 2.15 (br s, Nme_2, 24H), 3.24-3.41 (m, CH_2, 8H), 4.15 (s, 4H, Fc), 4.55 (s, 4H, Fc), 7.41-7.63 (m, ArH, 16H), 7.86-8.48 (m, Pyr-H, 16H). Anal. Calcd for $C_{112}H_{128}N_{12}P_4Fe_2Cu_4Br_4$: C, 54.87; H, 5.26; N, 6.86%. Found: C, 55.22; H, 5.34; N, 6.61%.

X-ray Crystallography

Crystals of each of the complexes **2** and **4** suitable for X-ray crystal analysis were mounted on a Cryoloop with a drop of Paratone oil and placed in the cold nitrogen stream of the Kryoflex attachment of the Bruker APEX CCD diffractometer. The diffraction data for both **2** and **3** were obtained from three sets of 400 frames, each of width 0.5° in ω, collected at ϕ = 0.00, 90.00 and 180.00° and two sets of 800 frames, each of width 0.45° in ϕ, collected at ω = –30.00 and 210.00°. The scan time was 20 sec/frame. The raw data were processed using the multi-component version of SAINT[27] under control of the two-component orientation file generated by CELL_NOW[28]. The raw data were reduced to F^2 values using the SAINT+ software[29]. Multiple measurements of equivalent reflections provided the basis for an empirical absorption correction as well as a

correction for any crystal deterioration during the data collection (SADABS)[30]. Reflections were merged by SHELXL according to the crystal class for the calculation of statistics and refinement. The structures **2** and **4** were solved by Patterson method and refined by full-matrix least-squares procedures using the SHELXL program package[31]. All esds (except the esd in the dihedral angle between two l.s. planes) are estimated using the full covariance matrix. The cell esds are taken into account individually in the estimation of esds in distances, angles and torsion angles; correlations between esds in cell parameters are only used when they are defined by crystal symmetry. An approximate (isotropic) treatment of cell esds is used for estimating esds involving l.s. planes. H-atoms attached to carbon were placed in calculated positions (C–H = 0.95 – 1.00 Å). All were included as riding contributions with isotropic displacement parameters 1.2 – 1.5 times those of the attached atoms. For **2** and **4**, density associated with disordered and partially occupied solvent molecule sites which were well-removed from the main molecule was removed with *PLATON SQUEEZE*[32]. The results indicated 184 electrons and a volume of 930 Å^3 for **2** and 195 electrons and a volume of 938 Å^3 for **4**. Crystallographic Data Centre as supplementary publication no. CCDC 2236366 (compound 2) and 2236367 (compound 4).

Results and Discussion

Treatment of ferrocenylbisphosphine [Fe{$C_5H_4P(C_6H_4CH_2NMe_2$-*o*)$_2$}$_2$] (**1**)with two equivalents of CuX (X = Cl, Br, I) in dichloromethane/acetonitrile resulted in the formation ofhalide bridged dinuclear complexes [{$Cu_2(\mu$-X)$_2$}{$Fe(C_5H_4P(C_6H_4CH_2NMe_2$-*o*)$_2$)$_2$}] (**2**,X= Cl;**3**, X= Br; **4**,X= I) in good yield, as shown in Scheme 1. The complexes **2** and **3** are soluble in polar solvents such as acetonitrile, dichloromethane and chloroform but insoluble in non-polar solvents. The ^{31}P NMR spectra of complexes **2** and **3** showed broad single resonances at δ –38.3 and –17.2, respectively, indicating the identical environment around phosphorus atoms. In the ^{1}H NMR spectra, complexes **2** and **3** showed single broad resonances at δ 4.58 and 4.75 for the ferrocenyl protons. In the ^{1}H NMR spectra, complex **3** showed two resonances at δ 1.70 and 2.42 for coordinated and un-coordinated NMe_2 groups, respectively. The complex **4** is insoluble in most of the organic solvents, as a result, NMR studies could not be carried out. The microanalysis data is found to be consistent with the proposed structures and the molecular structures of **2**and **4** are confirmed by the single crystal X-ray diffraction studies.

The dinuclear iodo-derivative [{$Cu_2(\mu$-I)$_2$}{$Fe(C_5H_4P(C_6H_4CH_2NMe_2$-*o*)$_2$)$_2$}] (**4**) was used for further reactions with strong Lewis bases, such as pyridine, 2,2′-bipyridine and 4,4′-bipyridine which resulted in the formation of several mixed ligand complexes as shown in Scheme 2. The reports of such type of mixed ligand copper(I) complexes containing both bisphosphines and aromatic amines are scarce[33,34]. Several groups have studied the copper(I) chemistry of numerous bridging diamine ligands such as piperazine, *N*,*N*′-dimethylpiperazine, 4,4′-bipyridyl[35,36], pyrazine[37-39], quinoxaline and 1,3,5-triazine[40]. The reaction of **4** with pyridine resulted in the formation of a binuclear complex, [{Cu_2I_2(py)$_2$}{$Fe(C_5H_4P(C_6H_4CH_2NMe_2$-*o*)$_2$)$_2$}] (**5**) (py = pyridine) in which each copper atom is tetracoordinated to phosphorus, one -NMe_2 group, one iodide and pyridine ligand (Scheme 2). The reaction was carried out in an excess of pyridine as the reaction did not proceed in acetonitrile or dichloromethane. The ^{31}P NMR spectrum of **5** showed a broad single resonance at δ –18.4. The ^{1}H NMR spectrum of **5** showed broad peaks at δ 7.64, 7.71 and 8.43, corresponding to the pyridyl protons. Similarly,

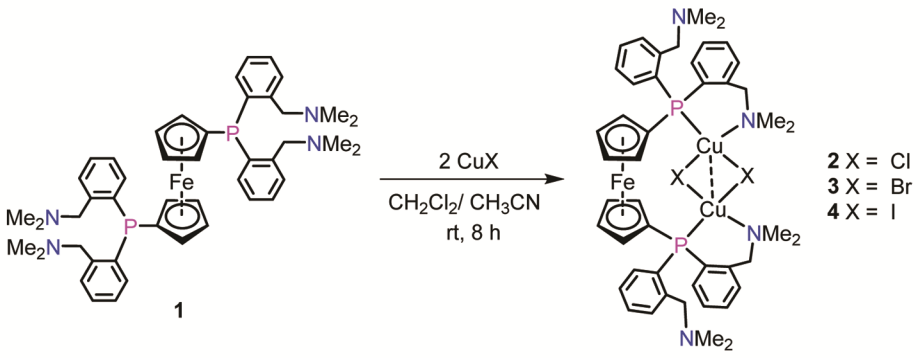

Scheme 1 — Synthesis of copper(I) complexes

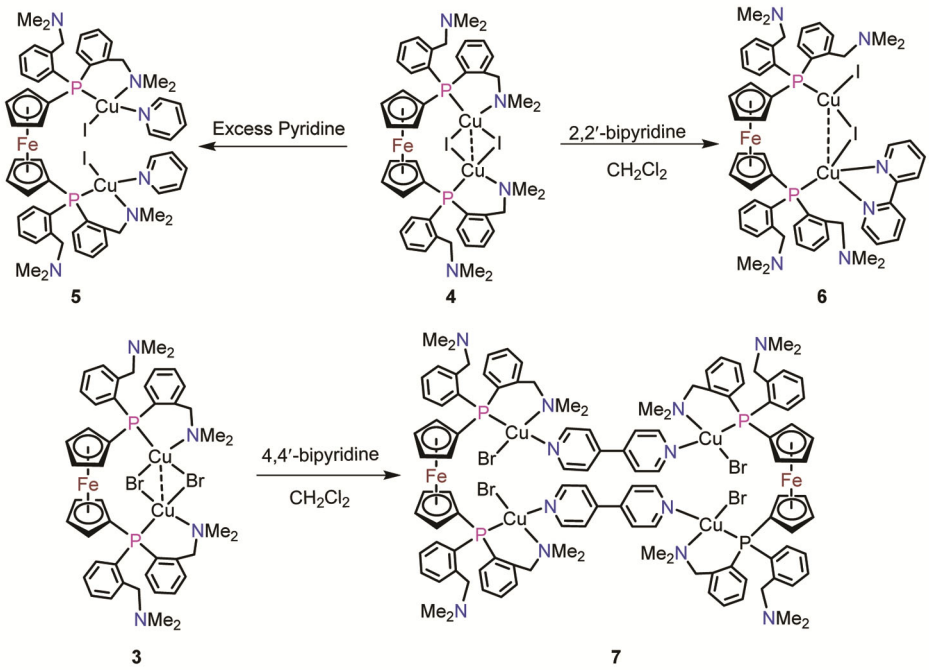

Scheme 2 — Synthesis of copper complexes

treatment of **4** with 2,2′-bipyridine in 1:1 molar ratio afforded the binuclear complex, [{Cu_2I_2(2,2′-bipy)}{Fe-($C_5H_4P(C_6H_4CH_2NMe_2$-*o*)$_2$)$_2$}] (**6**) (2,2′-bipy = 2,2′-bipyridine) as bright yellow crystalline solid. In complex **6**, one of the Cu-I bonds was cleaved by 2,2′-bipyridine to give both tri- and tetracoordinated copper centers. The ^{31}P NMR spectrum of complex **6** showed a broad single peak at δ –18.9. The ^{1}H NMR spectrum consists of two broad singlets in the region δ 4.05-4.77 for the ferrocenyl protons. The molecular compositions of **5** and **6** are verified by elemental analysis. The equimolar reaction of [{Cu_2(μ-Br)$_2$}{Fe($C_5H_4P(C_6H_4CH_2NMe_2$-*o*)$_2$)$_2$}] (**3**) and 4,4′-bipyridine afforded [{Cu_2Br_2(4,4′-bipy)}$_2$Fe($C_5H_4P(C_6H_4CH_2NMe_2$-*o*)$_2$)$_2$}$_2$] (**7**) as a pale yellow crystalline solid as shown in Scheme 2. In the ^{31}P NMR spectrum, the tetranuclear complex **7** showed a broad singlet at δ –13.9. The ^{1}H NMR and analytical data are consistent with the proposed structure of complex **7**.

Perspective views of the molecular structures of complexes **2** and **4** with the atom numbering schemes are shown in Fig. 1. The crystallographic data and the details of the structure determination are given in Table 1, while the selected bond lengths and bond angles are listed in Table 2. Complexes **2** and **4** crystallized in the monoclinic space group with C2/c. The molecular structures of complexes **2** and **4** are

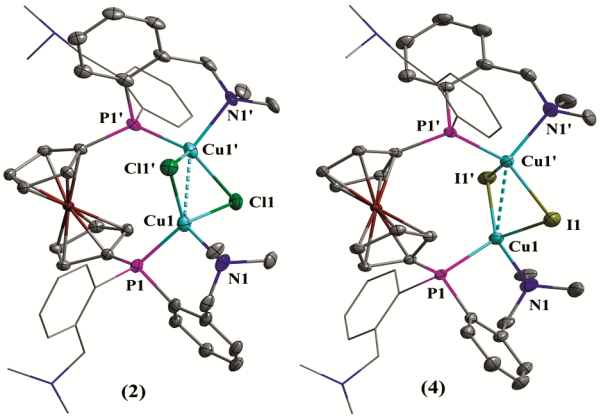

Fig. 1 — Molecular structures of **2** and **4**. All hydrogen atoms have been omitted for clarity. Displacement ellipsoids are drawn at the 50% probability level.

very similar to each other, consisting of Cu_2X_2 core having crystallographically-imposed centrosymmetry. Both complexes **2** and **4** are dinuclear with both the halide atoms (Cl, I) and the bisphosphine ligand bridging the two tetrahedral copper centers. The Cu_2X_2 core in **2** and **4** adopt a butterfly shape with the halide atoms at the wingtips. The distance between the two copper centers in **2** and **4** are 2.7258(9) Å and 2.8350(11) Å, respectively, which indicates the presence of ligand supported Cu···Cu interactions (Fig. 2). In the molecular structures of **2** and **4**, the two independent Cu-P distances differ only slightly

Table 1 — Crystallographic information for complexes **2** and **4**

	2	**4**
Empirical formula	$C_{46}H_{56}N_4P_2Cl_2FeCu_2$	$C_{46}H_{56}Cu_2FeI_2N_4P_2$
Formula weight	980.71	1163.61
Temperature/K	100(2)	100(2)
Crystal system	monoclinic	monoclinic
Space group	C2/c	C2/c
a/Å	21.259(3)	22.086(6)
b/Å	24.250(4)	23.767(7)
c/Å	9.7919(15)	9.834(3)
α/°	90	90
β/°	93.137(2)	92.224(4)
γ/°	90	90
Volume/Å^3	5040.4(13)	5158(3)
Z	4	4
ρ_{calc}g/cm^3	1.292	1.498
μ/mm^{-1}	1.323	2.386
F(000)	2032.0	2320.0
Crystal size/mm^3	0.207 × 0.177 × 0.088	0.278 × 0.089 × 0.078
Radiation	MoKα (λ = 0.71073)	MoKα (λ = 0.71073)
2θ range, deg	3.36 to 58.29	3.428 to 58.268
Reflections collected	45732	46917
Independent reflections	6693 [R_{int} = 0.0541]	6857 [R_{int} = 0.0515]
Data/restraints/parameters	6693/0/262	6857/0/262
Goodness-of-fit on F^2	1.060	1.044
R_1(I > 2σ(I))	0.0421	0.0403
wR_2(for all data)	0.1003	0.1135
Largest diff.peak/hole /eÅ^{-3}	0.81/–0.71	1.98/–1.69

Table 2 — Selected bond distances (Å) and bond angles (deg) for **2** and **4**

	2 (X =Cl1)	**4** (X = I1)
Selected bond distances (Å)		
Cu1–P1	2.1831(7)	2.2278(10)
Cu1–N1	2.165(2)	2.201(3)
Cu1–X	2.3110(8)	2.6047(7)
Cu1–X′	2.4268(8)	2.6672(9)
Cu1–Cu1′	2.7259(7)	2.8351(10)
Selected bond angles (deg)		
Cu1–X–Cu1′	70.20(2)	65.05(2)
X–Cu1–Cu1′	56.89(2)	58.54(2)
X–Cu1–X′	103.68(2)	108.25(2)
X′–Cu1–Cu1′	52.908(19)	56.411(16)
N1–Cu1–P1	98.45(7)	96.82(9)
P1–Cu1–X′	110.40(2)	110.67(2)
N1–Cu1–X	105.14(7)	105.85(10)

(Cu1-P1 = 2.1831(7) Å for **2** and Cu1-P1 = 2.2278(10) Å for **4**) while the X-Cu-X′ angles (Cl1-Cu1-Cl1′ = 103.68(2)° for **2** and I1-Cu1-I1′ = 108.25(2)° for **4**) show the distortion in the tetrahedral environment around copper atoms. The angles around the halide atoms: Cu-X-Cu′(Cu1-Cl1-Cu1′ = 70.20(2)° for **2** and Cu1-I1-Cu1′ = 65.05(2)° for **4**)

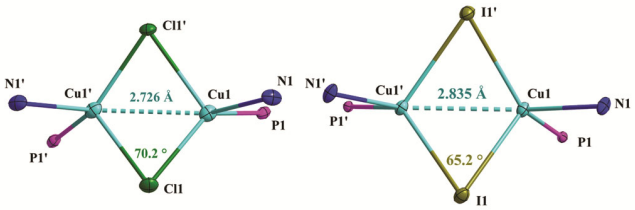

Fig. 2 — Pictographic represents of Cu···Cu′ distance and Cu–X–Cu′ angles of **2** (left) and **4** (right).

are considerably smaller. In complexes **2** and **4** the cyclopentadienyl rings adopt staggered conformation.

In the crystal packing of complex **2**, inversion-related C9–H9···Cl1^i intermolecular hydrogen bonds involving an aromatic proton of phenyl ring from the moiety that coordinated to Cu center and one of the Cl of $Cu_2(\mu\text{-}Cl)_2$ moiety (H9···Cl1^i= 2.943 Å), forming chains of molecules which propagate, respectively, along *a*-axis direction (Table 3 and Fig. 3). The inversion-related C–H···π(ring) interactions involving an aromatic ring proton of phenyl ring ($C_6H_4CH_2NMe_2$-*o*) that coordinated with Cu center and the centroid (Cg1) of the C15–C20 ring at 1/2-x,1/2-y, 1-z (H8···Cg1 = 2.931 Å and C8–H8···Cg1 = 154°), holding the two different layers that propagate

along *a*-axis direction (Table 3 and Fig. 4). The layers are also stacked with additional inversion-related C–H···π(ring) interactions involving a methyl proton of un-coordinated -CH_2NMe_2 group to Cu atom and the centroid (Cg2) of the C1–C5 ring at x, 1-y, 1/2+z (C22B···Cg2 = 3.144 Å and C22-C22B···Cg2 = 138°), forming a three-dimensional array of molecules (Table 3 and Fig. 4). The crystal packing also reveals numerous H···H contacts throughout the crystal packing: contacts involve (i) methyl proton of coordinated and un-coordinated NMe_2 groups to Cu center (H13C···H23C = 2.373 Å, 0.027 Å less than the sum of the van der Waals radii; symmetry code: 1/2-x, 1/2-y, 1-z) and (ii) an aromatic proton of one of the phenyl rings ($C_6H_4CH_2NMe_2$-*o*) and methyl proton of coordinated NMe_2 group to Cu center (H10···H14C = 2.373 Å, 0.027 Å less than the sum of the van der Waals radii; symmetry code: 1/2+x, 1/2-y, 1/2+z), as shown in Table 3 and Fig. 3.

Table 3 — Hydrogen-bond geometry (Å, °) for **2**. Cg1 is the centroid of the C15–C20phenyl ring and Cg2 is the centroid of the C1–C5Cpring.

D–H···*A*	*D*–H	H···*A*	D···*A*	*D*–H···*A*
C9-H9···Cl1[i]	0.95	2.943	3.873	166
C8-H8···Cg1[ii]	0.95	2.931	3.871	171
C22-C22B···Cg2	0.98	3.144	3.928	138

(i) 1/2+x,1/2-y, 1/2+z; (ii) 1/2-x,1/2-y, 1-z; (iii) x, 1-y, 1/2+z.

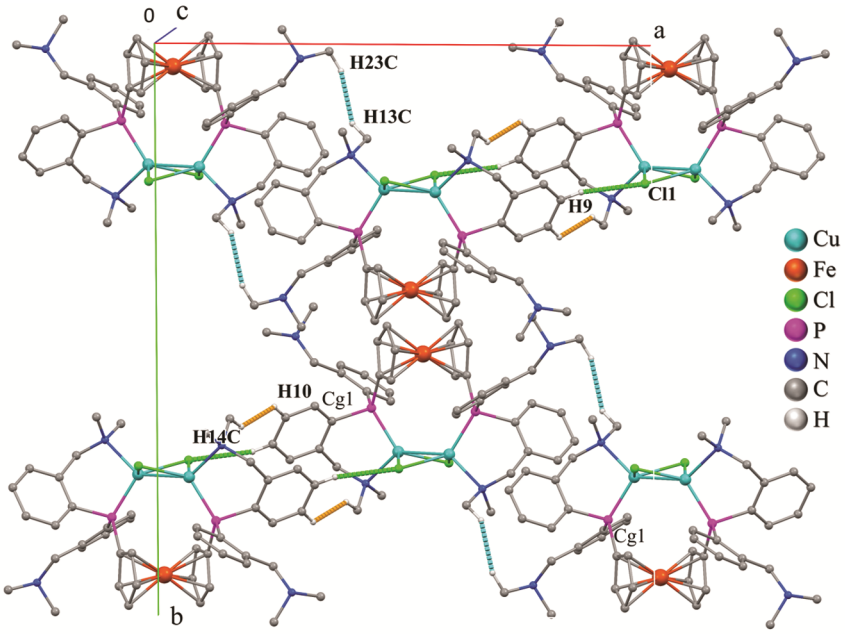

Fig. 3 — Packing diagrams showing the two-dimensional arrangement of complex **2** involving: (i) intermolecular C–H···Cl interactions (green dotted lines) and(ii) H···Hcontacts (greenish-blue and orange dotted lines).

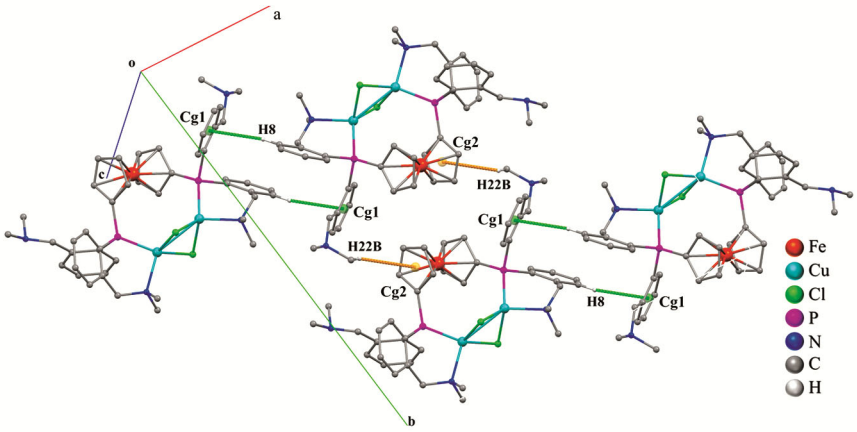

Fig. 4 — Packing diagrams showing the two-dimensional arrangement of complex **2** involving intermolecular C–H···π(ring) interaction (greenand orange dotted lines).

Table 4 — Hydrogen-bond geometry (Å, °) for **4**. Cg3 is the centroid of the C1–C5 Cp ring.

D–H···*A*	*D*–H	H···*A*	D···*A*	*D*–H···*A*
C9-H9···I1^{i}	0.95	3.102	4.024	164
C22-C22C···Cg3^{ii}	0.98	3.177	3.946	137

(i) –1/2+x,1.5-y, –1/2+z; (ii) x,1-y, –1/2+z.

In the crystal packing of complex **4**, unlike complex **2** inversion-related C9–H9···I1^{i} intermolecular hydrogen bonds involving an aromatic proton of phenyl ring from the moiety that coordinated to Cu center and one of the iodide of $Cu_2(\mu\text{-}I)_2$ moiety (H9···I1^{i}= 3.102 Å), forming chains of molecules which propagate along *a*-axis direction

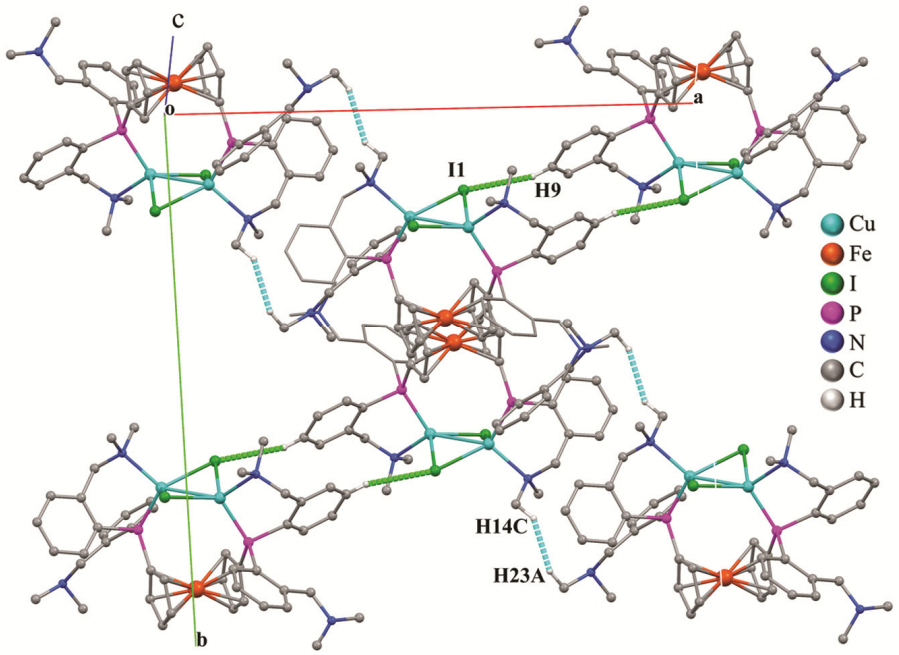

Fig. 5 — Packing diagrams showing the two-dimensional arrangement of complex **4** involving: (i) intermolecular C–H···I interactions (green dotted lines) and(ii) H···Hcontacts (greenish-blue dotted lines).

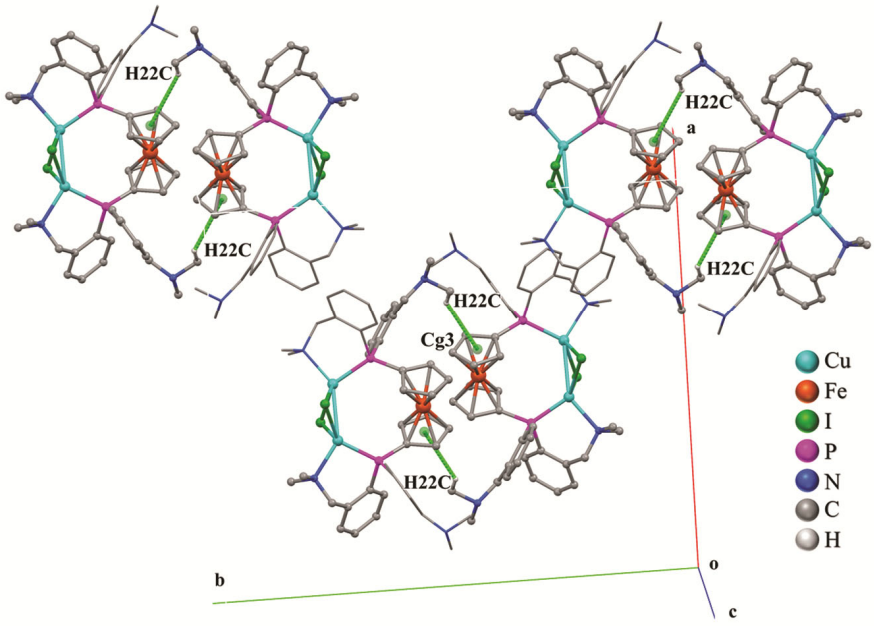

Fig. 6 — Packing diagrams showing the two-dimensional arrangement of complex **2** involving intermolecular C–H···π(ring) interaction (greenand orange dotted lines).

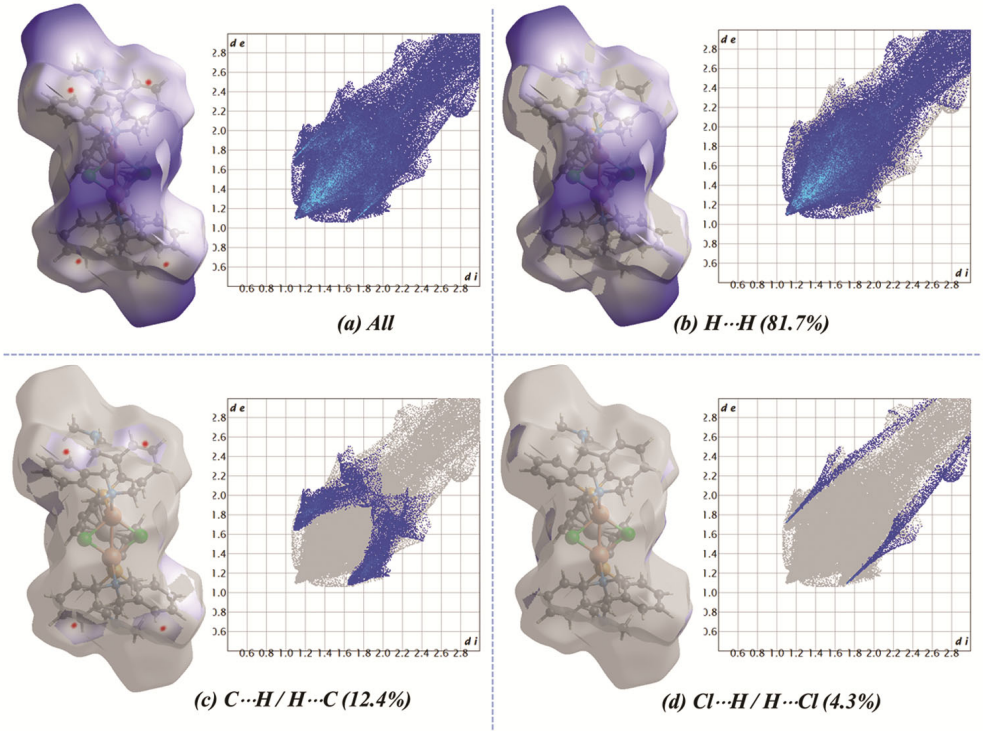

Fig. 7 — Hirshfeld surface of **2** mapped with (i) d_{norm} (left images of each pair) and (ii) a view of the two-dimensional fingerprint plots (right images of each pair), showing (a) all interactions, and delineated into (b) H···H, (c) C···H/H···C and (d) Cl···H/H···Clinteractions. The d_i and d_e values are the closest internal and external distances (in Å) from given points on the Hirshfeld surface.

(Table 4 and Fig. 5). The layers are stacked by inversion-related C–H···(ring) interactions involving a methyl proton of un-coordinated -CH_2NMe_2 group to Cu atom and the centroid (Cg3) of the C1–C5ring at x, 1-y, -1/2+z (C22C···Cg3 = 3.177 Å and C22-C22C···Cg3 = 137°) holding the layers that propagate along *a*-axis direction (Table 4 and Fig. 6). The crystal packing also reveals the presence of H···H contacts throughout the crystal packing: contacts involving methyl proton of coordinated and uncoordinated NMe_2 groups to Cu center (H14C···H23A = 2.278 Å, 0.122 Å less than the sum of the van der Waals radii; symmetry code: 1.5-x, 1.5-y, 1-z), as shown in Fig. 5.

Hirshfeld Surface Analysis

In order to visualize the intermolecular interactions in the crystals of complexes **2** and **4**, a Hirshfeld surface (HS) analysis[41] and the associated two-dimensional fingerprint plots[42] were carried out using Crystal Explorer 21.5[43]. A view of the three-dimensional Hirshfeld surface of all title complexes (**2**and **4**) plotted over d_{norm} using a "high standard" surface resolution colour-mapped over the normalized contact distance. The default setting used for Hirshfeld Surface/fingerprint generation in Crystal Explorer is: Isovalue: 0.5; property: none; resolution: High (standard). For fingerprint generation (d_i *vs* d_e plot); range: expanded, filter: by elements and fingerprint filter options are both inside-outside elements including reciprocal contacts. The red, white and blue regions visible on the d_{norm} surfaces indicate contacts with distances shorter, longer and equal to the van der Waals separations, respectively (Fig. 7 and Fig. 8). In complex **2**, the overall two-dimensional fingerprint plot, and those delineated into H···H (81.7%), C···H/H···C (12.4%), Cl···H/H···Cl (4.3%), N···H/H···N (0.8%) and C···C(0.9%) contacts are illustrated in Fig. 7. The large number of H···H, C···H/H···C and Cl···H/H···Cl interactions suggest that van der Waals interactions and hydrogen bonding play major roles in crystal packing. Similarly in complex **4**, the overall two-dimensional fingerprint plot, and those delineated into H···H (80.9%), C···H/H···C (12.1%), I···H/H···I (5.4%), N···H/H···N (0.9%) and C···C (0.7%) contacts are illustrated in Fig. 8. The large number of H···H, C···H/H···C and I···H/H···I interactions suggest that van der Waals interactions and hydrogen bonding play major roles in crystal packing.

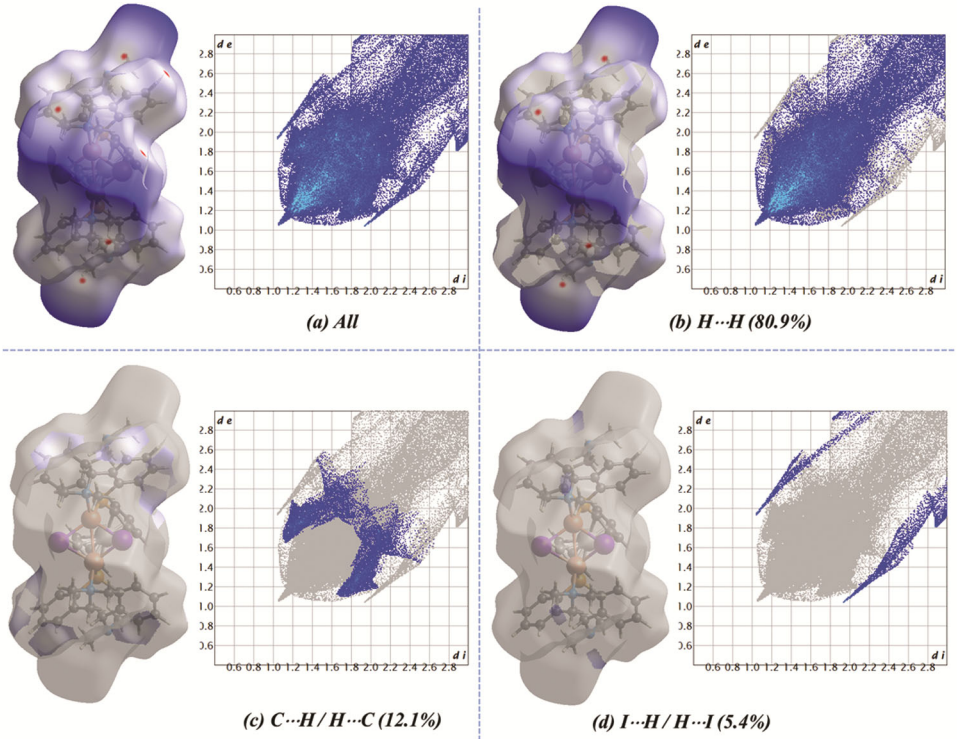

Fig. 8 — Hirshfeld surface of **4** mapped with (i) d_{norm} (left images of each pair) and (ii) a view of the two-dimensional fingerprint plots (right images of each pair), showing (a) all interactions, and delineated into (b) H···H, (c) C···H/H···C and (d) I···H/H···Iinteractions. The d_i and d_e values are the closest internal and external distances (in Å) from given points on the Hirshfeld surface.

Conclusions

Copper(I) complexes with ferrocenylbisphosphine were synthesized and structurally characterized. Copper complexes adopted Cu_2X_2 rhombic units to form dinuclear Cu(I) complexes. Addition of pyridine and 2,2′-bipyridine, resulted in breaking halo-bridges to form the mixed ligand complexes. The reaction of 4,4′-bipyridine with CuBr-complex afforded 4,4′-bipyridine bridged tetra-nuclear complex. The dissimilarity in Cu···Cu bond distances of Cu(I)complexes can be attributed to the difference in the size of halide ions.

Supplementary Information

Supplementary information is available in the website http://nopr.niscpr.res.in/handle/123456789/58776.

Acknowledgements

The authors are grateful to the Science and Engineering Research Board, New Delhi, for financial support of this work through grant CRG/2019/000040. The authors also thank the Department of Chemistry Instrumentation Facilities, IIT Bombay, for spectral and analytical data. DM thanks the Department of Science and Technology, New Delhi, for an Inspire fellowship. JTM thanks the Louisiana Board of Regents for the purchase of the CCD diffractometer and the Chemistry Department of Tulane University for support of the X-ray laboratory.

References

1 Paderina A V, Koshevoy I O & Grachova E V, *Dalton Trans*, 50 (2021) 6003.
2 Balakrishna M S, Copper(I) Chemistry of Phosphines, Functionalized Phosphines and Phosphorus Heterocycles, Balakrishna M S Ed, (Elsevier) 2019.
3 Pandey M K, Kunchur H S, Ananthnag G S, Mague J T & Balakrishna M S, *Dalton Trans*, 48 (2019) 3610.
4 Ananthnag G S, Mague J T & Balakrishna M S, *Dalton Trans*, 44 (2015) 3785.
5 Siddiqui M M, Mobin S M, Senkovska I, Kaskel S & Balakrishna M S, *Chem Commun*, 50 (2014) 12273.
6 Rashid A, Ananthnag G S, Naik S, Mague J T, Panda D & Balakrishna M S, *Dalton Trans*, 43 (2014) 11339.
7 Balakrishna M S, Suresh D, Ananthnag G S & Mague J T, *Dalton Trans*, 43 (2014) 8835.
8 Balakrishna M S, Suresh D, Rai A, Mague J T & Panda D, *Inorg Chem*, 49 (2010) 8790.
9 Ananthnag G S, Mague J T & Balakrishna M S, *Inorg Chem*, 54 (2015) 10985.
10 Siddiqui M M, Mague J T & Balakrishna M S, *Inorg Chem*, 54 (2015) 6063.
11 Radhakrishna L, Kunchur H S, Namdeo P K, Butcher R J & Balakrishna M S, *Dalton Trans*, 49 (2020) 3434.

12 Kumar S, Mondal D & Balakrishna M S, *ACS Omega*, 3 (2018) 16601.
13 Radhakrishna L, Pandey M K & Balakrishna M S, *RSC Adv*, 8 (2018) 25704.
14 Kumaravel M, Kumar P & Balakrishna M S, *J Chem Sci*, 126 (2014) 711.
15 Kunchur H S, Radhakrishna L, Pandey M K & Balakrishna M S, *Chem Commun*, 57 (2021) 4835.
16 Radhakrishna L, Kote B S, Kunchur H S, Pandey M K, Mondal D & Balakrishna M S, *Dalton Trans*, 51 (2022) 5480.
17 Namdeo P K, Sheokand S, Kote B S, Radhakrishna L, Kunchur H S, Saini P, Ramakrishnan S & Balakrishna M S, *Dalton Trans*, 51 (2022) 6795.
18 Kunchur H S & Balakrishna M S, *Inorg Chem*, 61 (2022) 857.
19 Rao S, Mague J T & Balakrishna M S, *Dalton Trans*, 42 (2013) 11695.
20 Prasad P S & Balakrishna M S, *J Organomet Chem*, 862 (2018) 31.
21 Sameer Prasad P, Pandey M K & Balakrishna M S, *Polyhedron*, 158 (2019) 173.
22 Siddiqui M M, Radhakrishna L, Mague J T & Balakrishna M S, *J Organomet Chem*, 824 (2016) 15.
23 Punji B, Mague J T & Balakrishna M S, *Inorg Chem*, 46 (2007) 10268.
24 Kunchur H S, Mondal D, Rao S, Mague J T & Balakrishna M S, *Acta Crystallogr C Struct Chem*, 77 (2021) 725.
25 Mondal D, Rao S, Mague J T & Balakrishna M S, *J Chem Crystallogr,* (2022) 273 https://doi.org/10.1007/s10870-022-00966-w.
26 Furniss B S, Hannaford A J, Smith P W G & Tatchell A R, *Vogel's Textbook of Practical Organic Chemistry, Fifth Edition,* (ELBS, England) 1989 p. 428.
27 Bruker, *APEX2, SADABS, SAINT & SHELXTL*, (Madison, WI) 2015.
28 Sheldrick G M, *CELL NOW*, (University of Göttingen, Göttingen, Germany) 2008.
29 Bruker, *APEX2*, version 2008.6-1, 2009.5-1, 2009.9-0, 2009.11-0, 2010.11-3; Bruker-AXS: Madison, WI, (2008, 2009a).
30 Sheldrick G M, *SADABS*, version 2008/2 and version 2009/2; University of Göttingen, Germany, (2008a, 2009).
31 Sheldrick G M, *SHELXS* and *SHELXL*,*Acta Cryst*, A64 (2008) 112.
32 Spek A, *Acta Cryst* C Struct Chem, 71 (2015) 9.
33 McCormick T, Jia W-L & Wang S, *Inorg Chem*, 45 (2006) 147.
34 Kuang S-M, Cuttell D G, McMillin D R, Fanwick P E & Walton R A, *Inorg Chem*, 41 (2002) 3313.
35 Yaghi O M & Li G, *Angew Chem Int Ed Engl*, 34 (1995) 207.
36 Lu J Y, Cabrera B R, Wang R-J & Li J, *Inorg Chem*, 38 (1999) 4608.
37 Li R-Z, Li D, Huang X-C, Qi Z-Y & Chen X-M, *Inorg Chem Commun*, 6 (2003) 1017.
38 Pike R D, Borne B D, Maeyer J T & Rheingold A L, *Inorg Chem*, 41 (2002) 631.
39 Maeyer J T, Johnson T J, Smith A K, Borne B D, Pike R D, Pennington W T, Krawiec M & Rheingold A L, *Polyhedron*, 22 (2003) 419.
40 Gustafsson B, Hakansson M & Jagner S, *Inorg Chim Acta*, 358 (2005) 1309.
41 Spackman M A & Jayatilaka D, *Cryst Eng Comm*, 11 (2009) 19.
42 McKinnon J J, Jayatilaka D & Spackman M A, *Chem Commun*, (2007) 3814. (https://doi.org/10.1039/B704980C).
43 Turner M J, McKinnon J J, Wolff S K, Grimwood D J, Spackman P R, Jayatilaka D & Spackman M A, (2017).